Int. J. Electrochem. Sci., 15 **(2020)** 2101 – 2114, doi: 10.20964/2020.03.68

International Journal of
ELECTROCHEMICAL
SCIENCE
www.electrochemsci.org

Effect of Cerium Substitution on Structural and Electrochemical Performance of $Li[Li_{0.2}Mn_{0.54}Co_{0.13}Ni_{0.13}]O_2$ Cathode Material for Lithium-Ion Battery

Zhaojun Tian, Yi Lu[*]

Hunan University of Science and Technology, School of Resource, Environment and Safety Engineering, Xiangtan, Hunan 411201
[*]E-mail: luyi-hnust@foxmail.com

Received: 14 November 2019 / *Accepted:* 2 January 2020 / *Published:* 10 February 2020

To enhance the cyclic stability and high rate performance of the advanced Lithium-rich and manganese-based layered structure cathode materials, the $Li_{1.20}[Mn_{0.54-x}Ni_{0.13}Co_{0.13}Ce_x]\ O_2$ (x = 0, 0.01, 0.02, 0.03) were synthesized by partially substituting Mn^{4+} with different amounts of Ce^{3+} via the traditional co-precipitation method. The effect of Ce^{3+} doping on the crystal structure, particles morphology and electrochemical properties of the $Li_{1.20}[Mn_{0.54}Co_{0.13}Ni_{0.13}]O_2$ was studied by X-ray diffraction (XRD), scanning electron microscope (SEM), galvanostatic charge-discharge tests and electrochemical impedance spectroscopy (EIS) measurement. The XRD, SEM and EDS results demonstrated that the cathodes after Ce^{3+} doping delivered the larger crystal lattice parameters, the lower cation mixing between Ni^{2+} and Li^{+} and the smaller size of cathode particles. Therefore, the superior rate capacity and cyclic performance were obtained for the Ce^{3+} doped cathodes. Particularly, the $Li_{1.20}[Mn_{0.52}Ni_{0.13}Co_{0.13}Ce_{0.02}]O_2$ demonstrated the optimal electrochemical properties, which delivered a high discharge capacity of 136.7 $mAhg^{-1}$ at 5C high rate and a high capacity retention of 91.2% at 2C rate after 100 cycles. While the pristine cathode only exhibited a discharge capacity of 92.8 $mAhg^{-1}$ at 5C rate, 43.9 $mAhg^{-1}$ smaller than that of the $Li_{1.20}[Mn_{0.52}Ni_{0.13}Co_{0.13}Ce_{0.02}]O_2$. In addition, it retained a discharge capacity of 112.3 $mAhg^{-1}$ with a capacity retention of only 81.5% after 100 cycles at 2C rate. The larger capacity retention and superior rate performance of Ce^{3+} doped cathodes could be ascribed to the fast Li^{+} diffusing speed, the high cation ordering and lower charge transfer resistance during cycling.

Keywords: $Li_{1.20}[Mn_{0.54}Co_{0.13}Ni_{0.13}]O_2$; Rare earth; Cerium doping; High rate capacity; Long-life cycle performance

1. INTRODUCTION

Since the Lithium ion battery was firstly manufactured by Sony in 1991, it has been widely applied in people daily life and industrial production due to the long cycling life and portability [1-3]. However, with the upgrade of electronic products, the traditional cathode materials cannot meet the

demand of high energy density [4-7]. Recently, the lithium-rich and manganese-based layered structure cathode materials xLi$_2$MnO$_3$·(1-x)LiMO$_2$ (M = Ni, Co, Mn) have attracted much attention for that they can deliver a high discharge capacity of 280mAh g^{-1}, which will be an competitive candidate for the cathode of next high-energy density Lithium-ion battery [8, 9]. After extensively studies, people have found that the poor rate capacity and severe capacity fading have restricted the widely applications of the lithium-rich and manganese-based layered structure cathode materials. The poor rate capacity of xLi$_2$MnO$_3$·(1-x)LiMO$_2$ (M = Ni, Co, Mn) may be connected with the low lithium ions migration rate and the severe capacity fading can be attributed to the structure instability during cycling [10, 11]. To solve the intrinsic drawbacks, various strategies, including ion doping, surface coating and synthetic method modification, have all been adopted [12-14]. Among the above methods, the ion doping has demonstrated the remarkable results on enhancing the rate performance and maintaining the structure stability during cycling [15]. For the doping components, the rare earth elements are particularly suitable for doping modification due to the chemical inertness and outstanding structure stability under harsh environmental conditions [16]. Besides, the compounds containing Cesium have widely adopted to cover on the surface of the lithium-rich and manganese-based layered structure cathode materials and improve the electrochemical properties. W. Yuan et al synthesized the CeO$_2$ coated Li(Li$_{0.17}$Ni$_{0.2}$Co$_{0.05}$Mn$_{0.58}$)O$_2$ cathode materials and found that 1wt.% CeO$_2$ coated cathode demonstrated the excellent cycle performance and high-rate discharge capability [17]. In addition, C. Lu *et al* proposed CeF$_3$ to cover on the surface of Li$_{1.2}$Mn$_{0.54}$Ni$_{0.13}$Co$_{0.13}$O$_2$ and the CeF$_3$ coated sample delivered a capacity retention of 91.7% after 50 cycles, much larger than that (82.1%) of the pristine one [18]. According to the above discussion, the Ce^{3+}, as the typical rare earth elements, may present some particular effect on enhancing the electrochemical property of cathode when doped into xLi$_2$MnO$_3$·(1-x)LiMO$_2$ (M = Ni, Co, Mn).

In this study, the Cesium ion was chosen as the doping element to substitute at Mn sites of Li$_{1.20}$[Mn$_{0.54}$Co$_{0.13}$Ni$_{0.13}$]O$_2$. And the Li$_{1.20}$[Mn$_{0.54-x}$Ni$_{0.13}$Co$_{0.13}$Ce$_x$] O$_2$ (x = 0, 0.01, 0.02, 0.03) were synthesized through a typical co-precipitation, followed by a two-step high temperature sintering process. The structure, morphology and electrochemical properties of as-prepared samples were systematically studied to evaluate the effects of Ce^{3+} doping on the Li[Li$_{0.2}$Mn$_{0.54}$Co$_{0.13}$Ni$_{0.13}$]O$_2$.

2. EXPERIMENTAL

The Li$_{1.20}$[Mn$_{0.54-x}$Ni$_{0.13}$Co$_{0.13}$Ce$_x$] O$_2$ (x = 0, 0.01, 0.02, 0.03) were prepared by combination of the carbonate co-precipitation and solid state reaction, as is described in our previous work [19]. To prepare the [Mn$_{0.54-x}$Ni$_{0.13}$Co$_{0.13}$Ce$_x$](CO$_3$)$_{0.8}$ (x = 0, 0.01, 0.02, 0.03) precursor, the MnSO$_4$·H$_2$O, NiSO$_4$·6H$_2$O, CoSO$_4$·7H$_2$O and Ce(NO$_3$)$_3$·6H$_2$O with the property stoichiometric amounts were chosen as raw materials, NH$_3$·H$_2$O was served as chelating agent and Na$_2$CO$_3$ was acted as precipitant, respectively. Finally, the [Mn$_{0.54-x}$Ni$_{0.13}$Co$_{0.13}$Ce$_x$](CO$_3$)$_{0.8}$ (x = 0, 0.01, 0.02, 0.03) precursors and LiOH·H$_2$O powder were pre-heated at 500 ºC for 6h and annealed at 950 ºC for 12h in air to acquire the target cathode materials Li$_{1.20}$[Mn$_{0.54-x}$Ni$_{0.13}$Co$_{0.13}$Ce$_x$] O$_2$ (x = 0, 0.01, 0.02, 0.03).

The precise cation composition of Li$_{1.20}$[Mn$_{0.54-x}$Ni$_{0.13}$Co$_{0.13}$Ce$_x$] O$_2$ (x = 0, 0.01, 0.02, 0.03) was monitored by ICP-OES (Inductively Coupled Plasma Optical Emission Spectrometer, iCAP 6000). The

crystal structure of the cathode materials was identified by X-ray diffraction (XRD) using a Rigaku RINT2400 X-ray diffractometer with Cu k*a* radiation in the 2θ angular range from 10° to 80° at a scanning rate of 0.02° s^{-1}. The cathode particles morphology and composition of the samples were observed via scanning electron microscopy (SEM, Ultra 55, Zeiss) equipped with energy dispersive X-ray spectrometer (EDAX).

The electrodes were prepared by mixing 85 wt.% as-prepared samples, 10 wt.% acetylene black (conductive additive), and 5wt% polyvinylidene fluoride (PVDF, binder) in N-methyl-2-pyrrolidone (NMP) solvent to form a homogeneous slurry, followed by pasted onto the Al foil and punched into a circular disc with d = 12 mm after complete dried. Then the as-prepared cathode plate, metal lithium foils as anode, polypropylene micro-porous films (Celgard 2400) as separator were assembled in an argon-filled glove box to form the CR2025 coin cells, which were then injected by the electrolyte (1M $LiPF_6$ dissolved in EC/DMC at mass ratio of 1:1). The coin cells were charged and discharged between 2.0 and 4.8 V at various current rates (1C =250mA g^{-1}) with LAND CT-2001A instrument (Wuhan, China). Electrochemical impedance spectra (EIS) were carried out using a CHI660D electrochemical workstation in the frequency range from 10 mHz to100 kHz with an amplitude of 5 mV.

3. RESULTS AND DISCUSSION

3.1 Microstructure characterization

The elemental analysis of $Li_{1.20}[Mn_{0.54-x}Ni_{0.13}Co_{0.13}Ce_x]O_2$ (x = 0, 0.01, 0.02, 0.03) was carried out by using ICP technique to verify the chemical compositions, as is shown in Table 1. The results indicate that the average chemical compositions of the as-prepared cathodes are very close to the experimental design values, meaning the chemical compositions of synthesized samples have achieved the anticipative effect.

Table 1. The chemical compositions of $Li_{1.20}[Mn_{0.54-x}Ni_{0.13}Co_{0.13}Ce_x]O_2$ (x = 0, 0.01, 0.02, 0.03).

Sample	Theoretical molar proportion				Actual molar proportion			
	Mn	Ni	Co	Ce	Mn	Ni	Co	Ce
x = 0	0.540	0.130	0.130	0	0.541	0.128	0.131	0
x = 0.01	0.530	0.130	0.130	0.010	0.533	0.129	0.129	0.009
x = 0.02	0.520	0.130	0.130	0.020	0.518	0.131	0.131	0.020
x = 0.03	0.510	0.130	0.130	0.030	0.509	0.131	0.131	0.029

The XRD patterns of $Li_{1.20}[Mn_{0.54-x}Ni_{0.13}Co_{0.13}Ce_x]O_2$ (x = 0, 0.01, 0.02, 0.03) are shown in Fig.1. All samples have demonstrated the sharp XRD diffraction patterns, indicating the well crystallization has been formed. Besides, all the main peaks of as-prepared cathodes have been identified as a typical α-$NaFeO_2$ layered hexagonal structure with the space group of R-3m [20]. While some weak superlattice reflections located at 20°~25° correspond to the monoclinic (C2/m) structure, belonging to

Li_2MnO_3 phase [21]. In addition, the clear splitting of (006)/(012) and (018)/(110) indicate the formation of a well hexagonal layered structure for all cathodes [22].

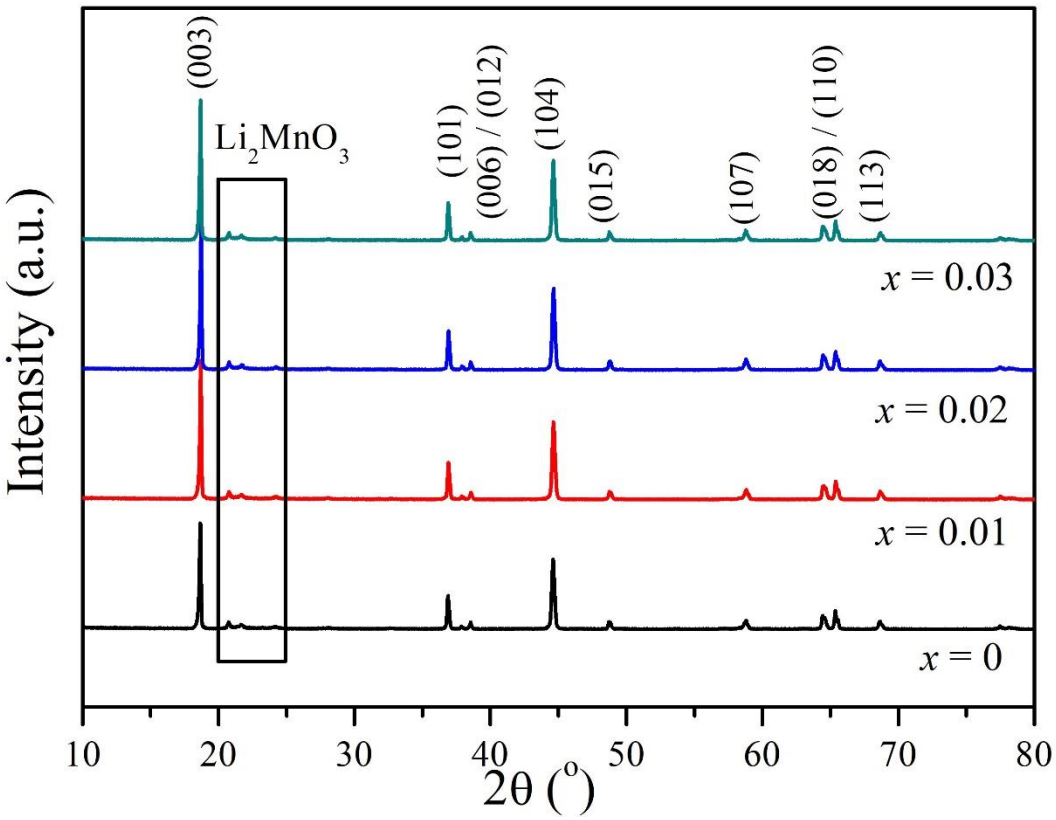

Figure 1. XRD patterns of the $Li_{1.20}[Mn_{0.54-x}Ni_{0.13}Co_{0.13}Ce_x]\ O_2$ (x = 0, 0.01, 0.02, 0.03).

Table 2. The crystallographic parameters of $Li_{1.20}[Mn_{0.54-x}Ni_{0.13}Co_{0.13}Ce_x]\ O_2$ (x = 0, 0.01, 0.02, 0.03).

Sample	*a*(Å)	*c*(Å)	*c*/*a*	*V*(Å^3)	$I_{(003)}/I_{(104)}$
x = 0	2.8475	14.2085	4.9898	98.56	1.56
x = 0.01	2.8491	14.2195	4.9909	99.87	1.63
x = 0.02	2.8525	14.2402	4.9922	100.03	1.78
x = 0.03	2.8536	14.2513	4.9941	100.32	1.68

Table 2 shows the crystallographic parameters of $Li_{1.20}[Mn_{0.54-x}Ni_{0.13}Co_{0.13}Ce_x]\ O_2$ (x = 0, 0.01, 0.02, 0.03). It can be observed that the parameters of *c* and *a* enlarge with the increase of Ce^{3+} doping amounts for that the ionic radius of Ce^{3+} (1.03 Å) is larger than that of Mn^{4+} (0.53 Å), which will contribute to enhancing the speed of Lithium ions migration. All samples deliver the high lattice parameter ratio of *c*/*a* (larger than 4.98), indicating the well layered structure have been obtained for the as-prepared cathodes [23]. Besides, the cathodes after Ce^{3+} doping have demonstrated the higher $I_{(003)}/I_{(104)}$ values than that of the pristine one, meaning the less cation mixing has occurred for the Ce^{3+} doped samples, which is help to enhance the structure stability [24].

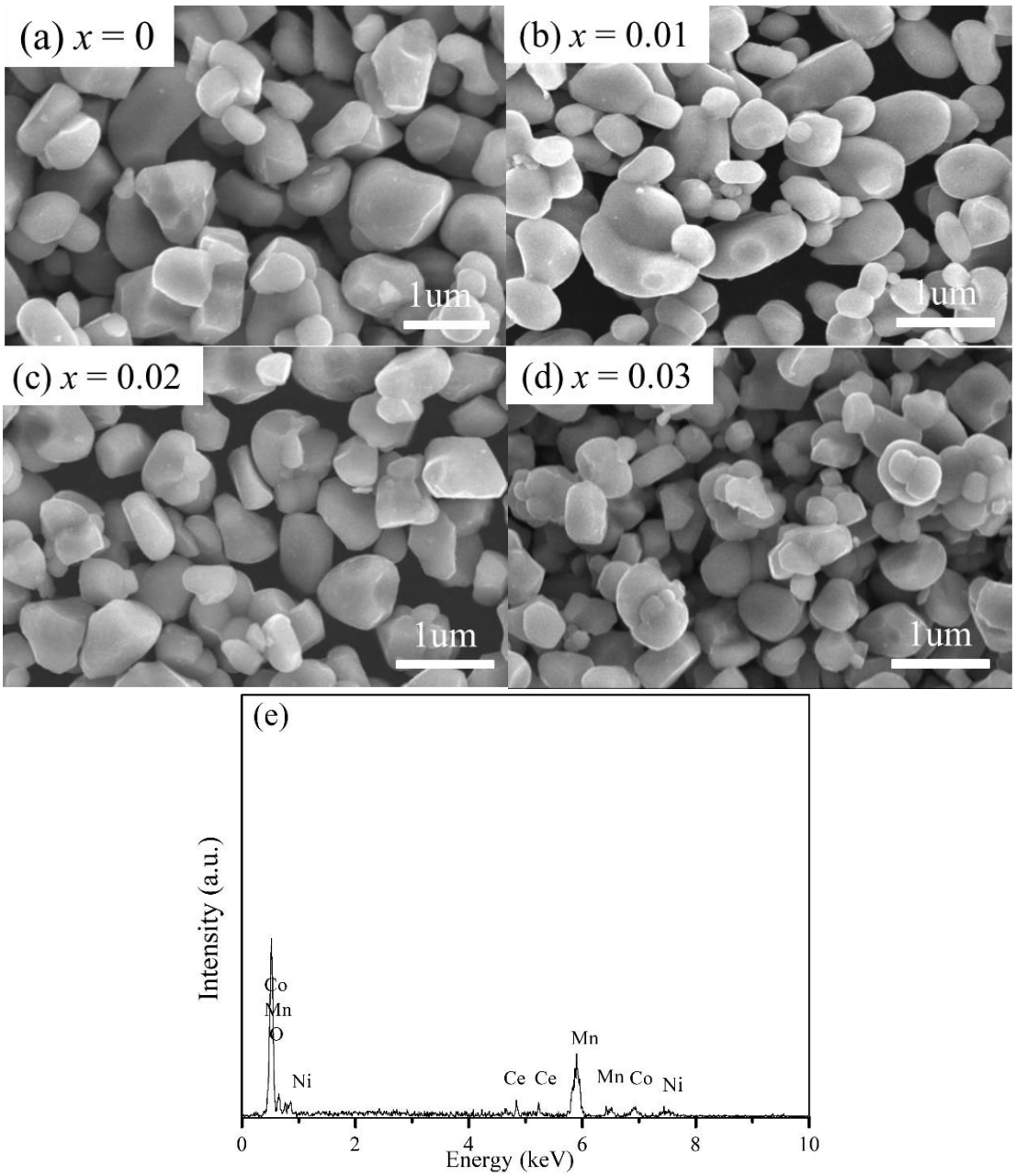

Figure 2. SEM images of $Li_{1.20}[Mn_{0.54-x}Ni_{0.13}Co_{0.13}Ce_x]\ O_2$ (x = 0, 0.01, 0.02, 0.03)(a~d); EDS spectrum of $Li_{1.20}[Mn_{0.52}Ni_{0.13}Co_{0.13}Ce_{0.02}]O_2$ (e).

The morphologies and sizes of the synthesized cathode particles will determine the electrochemical properties of as-prepared samples. Figure 2 shows the SEM images of $Li_{1.20}[Mn_{0.54-x}Ni_{0.13}Co_{0.13}Ce_x]\ O_2$ (x = 0, 0.01, 0.02, 0.03). The all cathode samples are consisted of abundant small spheroid grains with high crystallinity in a diameter size of 200~800nm. After the Ce^{3+} doping, no clear difference in cathode particles morphology can be observed. However, it can be observed that the Ce^{3+} doped cathodes have demonstrated the smaller size particles than that of the pristine one. And a smaller particle size can decrease the diffusion path of lithium ions, contributing to enhancing the high rate discharge performance. And Fig.2 (e) shows the EDS spectrum of $Li_{1.20}[Mn_{0.52}Ni_{0.13}Co_{0.13}Ce_{0.02}]O_2$, and

the elements of Mn, Ni, Co, Ce have all been detected, indicating the Ce^{3+} has successfully been doped into cathode.

3.2 Electrochemical behaviours

Fig.3 shows the initial charge and discharge profiles of $Li_{1.20}[Mn_{0.54-x}Ni_{0.13}Co_{0.13}Ce_x]\ O_2$ (x = 0, 0.01, 0.02, 0.03). Generally, the initial charging process can be divided into two steps, *i.e.* potential increasing region from 2.0~4.5V and a long potential plateau around 4.5V.

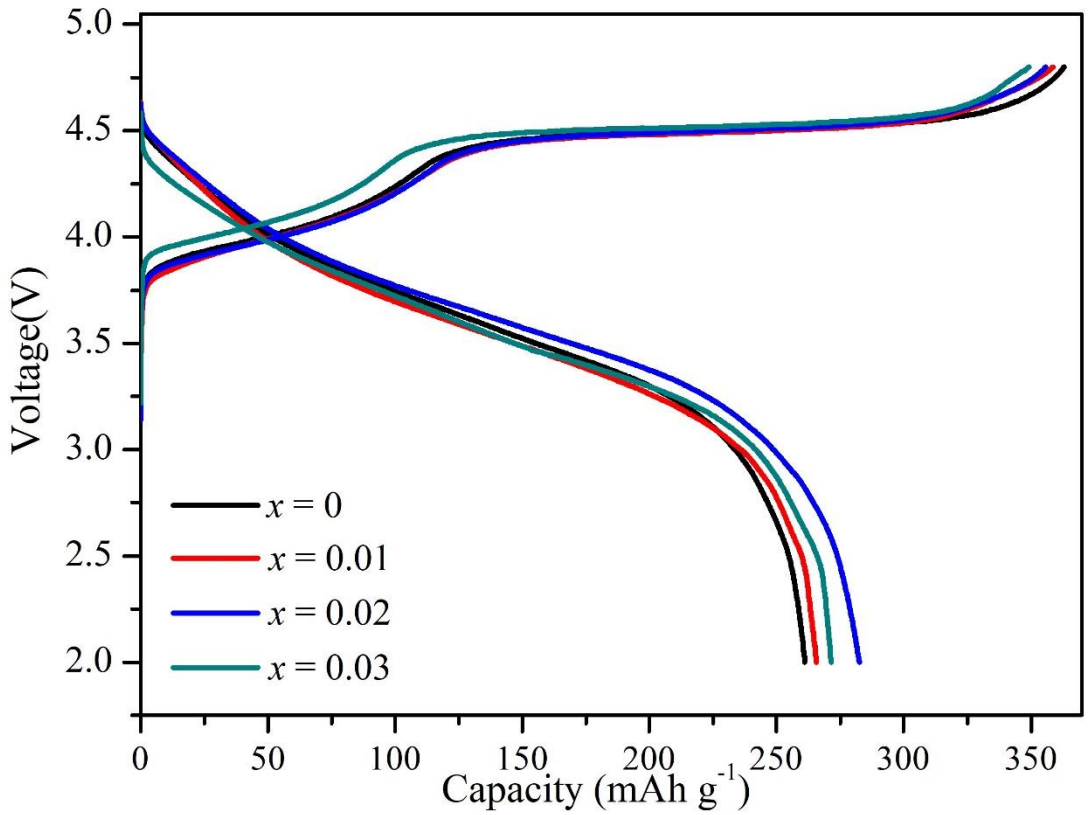

Figure 3. Initial charge and discharge profiles of $Li_{1.20}[Mn_{0.54-x}Ni_{0.13}Co_{0.13}Ce_x]\ O_2$ (x = 0, 0.01, 0.02, 0.03) in the voltage of 2.0~4.8V at 0.1 C rate.

The first step of charging profile is connected with the Li^+ extraction from the layered $LiMn_{1/3}Ni_{1/3}Co_{1/3}O_2$ component, accompanying with the oxidation of $Ni^{2+}\rightarrow Ni^{4+}$ and $Co^{3+}\rightarrow Co^{4+}$ [25]. In addition, the second step demonstrates the typical feature of the lithium-rich and manganese-based layered structure cathode materials, which corresponds to the irreversible loss of lattice oxygen as Li_2O removal from Li_2MnO_3 component [26]. And the loss of lattice oxygen will bring about the layered-to-spinel phase transformation of $xLi_2MnO_3\cdot(1-x)LiMO_2$ (M = Ni, Co, Mn), leading to the continuous capacity fade during cycling [27]. The relevant reaction equation of the above two charging steps can be described as follows:

$$LiMn_{1/3}Ni_{1/3}Co_{1/3}O_2\rightarrow Mn_{1/3}Ni_{1/3}Co_{1/3}O_2 + 0.4Li^+ + 0.4e^- \quad (1)$$

$$0.6Li_2MnO_3\rightarrow 0.6MnO_2 + 1.2Li^+ + 1.2e^- + 0.3O_2 \quad (2)$$

Table 3 delivers the initial charge and discharge capacities of $Li_{1.20}[Mn_{0.54-x}Ni_{0.13}Co_{0.13}Ce_x]\ O_2$ (x = 0, 0.01, 0.02, 0.03) at 0.1C rate in the voltage range of 2.0~4.8 V. It can be observed that the initial discharge capacity and the initial coulombic efficiency of Ce^{3+} doped cathodes are larger than those of the pristine one.

Table 3. Initial charge and discharge capacities of $Li_{1.20}[Mn_{0.54-x}Ni_{0.13}Co_{0.13}Ce_x]\ O_2$ (x = 0, 0.01, 0.02, 0.03) at 0.1C rate in the voltage range of 2.0~4.8 V.

Sample	Charge capacity (mAh g^{-1})	Discharge capacity (mAh g^{-1})	Irreversible capacity loss (mAh g^{-1})	Coulombic efficiency (%)
x = 0	362.9	261.1	101.8	71.9
x = 0.01	358.6	265.6	93.0	74.1
x = 0.02	355.8	282.4	73.4	79.4
x = 0.03	349.2	271.4	77.8	77.7

And with the Ce^{3+} doping amount increasing, the initial discharge capacities of $Li_{1.20}[Mn_{0.54-x}Ni_{0.13}Co_{0.13}Ce_x]\ O_2$ (x = 0, 0.01, 0.02, 0.03) are 261.1, 265.6, 282.4 and 271.4 mAh g^{-1}, corresponding to the charge-discharge coulombic efficiency of 71.9%, 74.1%, 79.4% and 77.7%, respectively. Obviously, the $Li_{1.20}[Mn_{0.52}Ni_{0.13}Co_{0.13}Ce_{0.02}]O_2$ delivers the highest initial discharge capacity and coulombic efficiency for that the Ce^{3+} doping can decrease the irreversible capacity loss during the first charging and discharging process. Since Ce–O possesses much higher bonding energy than Mn–O, and by partially substituting Mn^{4+} with a suitable amount of Ce^{3+} in $Li_{1.20}[Mn_{0.54}Ni_{0.13}Co_{0.13}]\ O_2$ can suppress the loss of lattice oxygen and stabilize the crystal structure [28]. However, the initial discharge capacity decline on the contrary when the Ce^{3+} doping amount further increases (up to 0.03). It maybe attributed to the decrease of cathode active material content.

Table 4. Discharge capacities of $Li_{1.20}[Mn_{0.54-x}Ni_{0.13}Co_{0.13}Ce_x]\ O_2$ (x = 0, 0.01, 0.02, 0.03) at different rates between 2.0~4.8V.

Sample	0.1C rate (mAh g^{-1})	0.2C rate (mAh g^{-1})	0.5C rate (mAh g^{-1})	1C rate (mAh g^{-1})	2C rate (mAh g^{-1})	5C rate (mAhg^{-1})	followed 0.1C rate
x = 0	263.5	235.6	198.2	162.3	135.9	92.8	244.0
x = 0.01	268.4	246.2	212.5	180.7	159.7	119.7	254.4
x = 0.02	285.3	262.9	232.8	203.5	176.8	136.7	277.6
x = 0.03	273.9	253.4	221.5	195.8	166.7	128.2	264.3

Rate capability is the key performance indicator of Lithium-ion battery for application of EVs and electric power tools. Fig.4 shows the rate capacities of $Li_{1.20}[Mn_{0.54-x}Ni_{0.13}Co_{0.13}Ce_x]\ O_2$ (x = 0, 0.01, 0.02, 0.03). All cathodes demonstrate that the discharge capacity will decrease with the current density increasing from 0.1C to 5C high rate, which is mainly attributed to the restriction of Li^+ migration speed, leading to the large voltage polarization. Fig.4(a)~(d) have demonstrated that the cathodes after Ce^{3+} doping have delivered the superior rate discharge capacities than those of the pristine one. Table 4

compares the specific discharge capacities of $Li_{1.20}[Mn_{0.54-x}Ni_{0.13}Co_{0.13}Ce_x]O_2$ (x = 0, 0.01, 0.02, 0.03) at the rates of 0.1C, 0.2C, 0.5C, 1C, 2C and 5C.

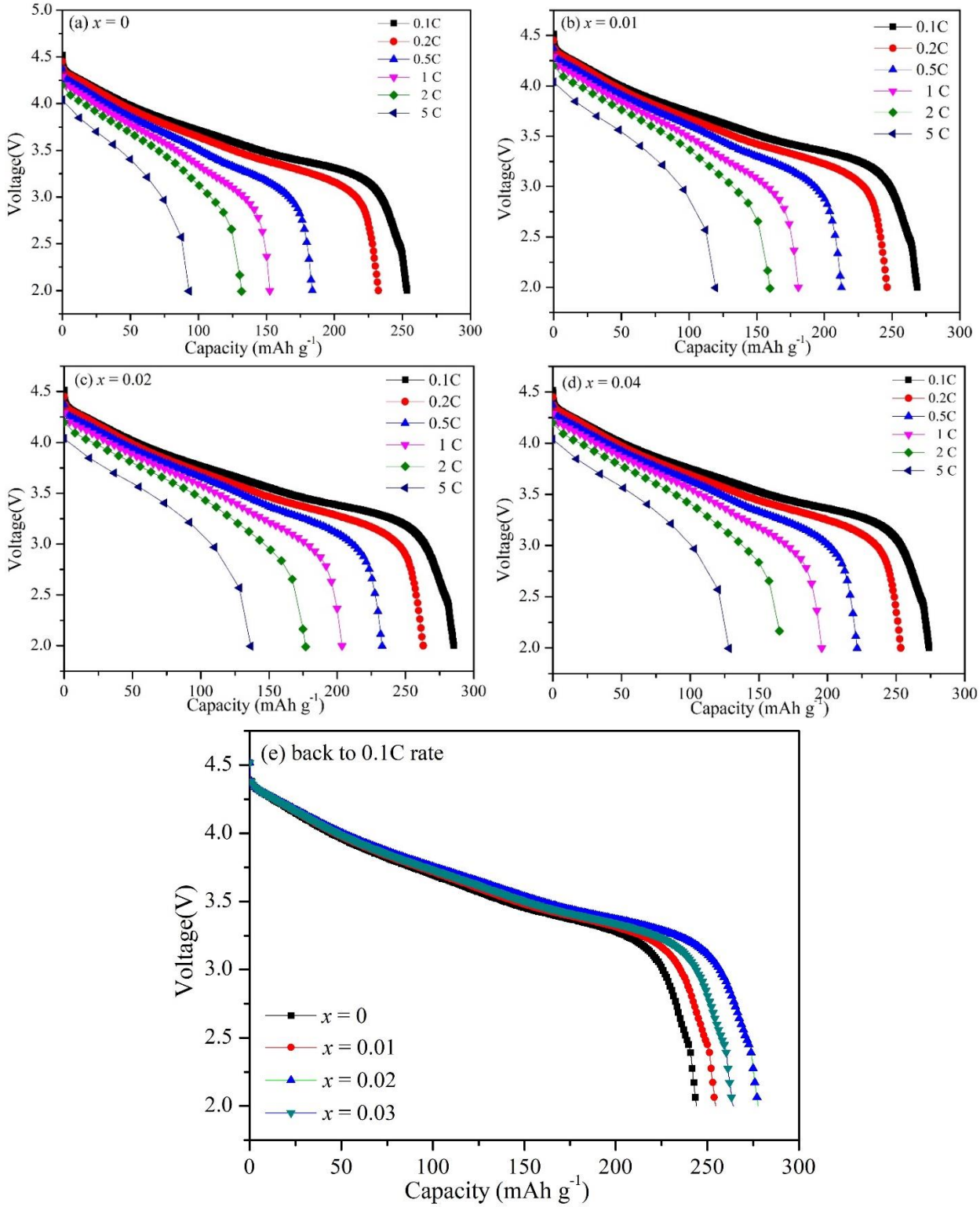

Figure 4. The initial discharge profiles of $Li_{1.20}[Mn_{0.54-x}Ni_{0.13}Co_{0.13}Ce_x]O_2$ (x = 0, 0.01, 0.02, 0.03) at a series of current densities.

Particularly, the $Li_{1.20}[Mn_{0.52}Ni_{0.13}Co_{0.13}Ce_{0.02}]O_2$ delivered the optimal rate performance among the four samples. The discharge capacities of $Li_{1.20}[Mn_{0.52}Ni_{0.13}Co_{0.13}Ce_{0.02}]O_2$ are respectively 285.3, 262.9, 232.8, 203.5, 176.8 and 136.7 $mAhg^{-1}$ at the rates of 0.1C, 0.2C, 0.5C, 1C, 2C and 5C. While the corresponding discharge capacities are 263.5, 235.6, 198.2, 162.3, 135.9 and 92.8 $mAhg^{-1}$ for the pristine one. It can be compared that the discharge capacity difference will enlarge when the current density increases. The $Li_{1.20}[Mn_{0.52}Ni_{0.13}Co_{0.13}Ce_{0.02}]O_2$ only delivers a higher discharge capacity of 21.8 $mAhg^{-1}$ than the pristine cathode at 0.1C rate. And when the current density increases to 5C high rate, the discharge capacity difference gap has been amplified to 43.9 mAh g^{-1}. The superior rate performance can be attributed to the larger lattice parameter caused by Ce^{3+} doping, which makes Li^+ move more quickly in the cathode particles. Besides, the formation of small size cathode particles for the Ce^{3+} doped samples can also improve the rate capability owing to the short migration path. Fig.4(e) shows the discharge capacities of $Li_{1.20}[Mn_{0.54-x}Ni_{0.13}Co_{0.13}Ce_x]$ O_2 (x = 0, 0.01, 0.02, 0.03) when cycled at 0.1 C rate again. The $Li_{1.20}[Mn_{0.54-x}Ni_{0.13}Co_{0.13}Ce_x]$ O_2 (x = 0, 0.01, 0.02, 0.03) deliver the discharge capacities of 244.0, 254.4, 277.6 and 264.3 mAh g^{-1}, respectively, corresponding to the capacity retention of 92.6%, 94.8%, 97.3%, and 96.5%. The result indicates that the Ce^{3+} doping is favorable to improve the reversibility of Lithium ions migration across the cathode/electrolyte interface during cycling.

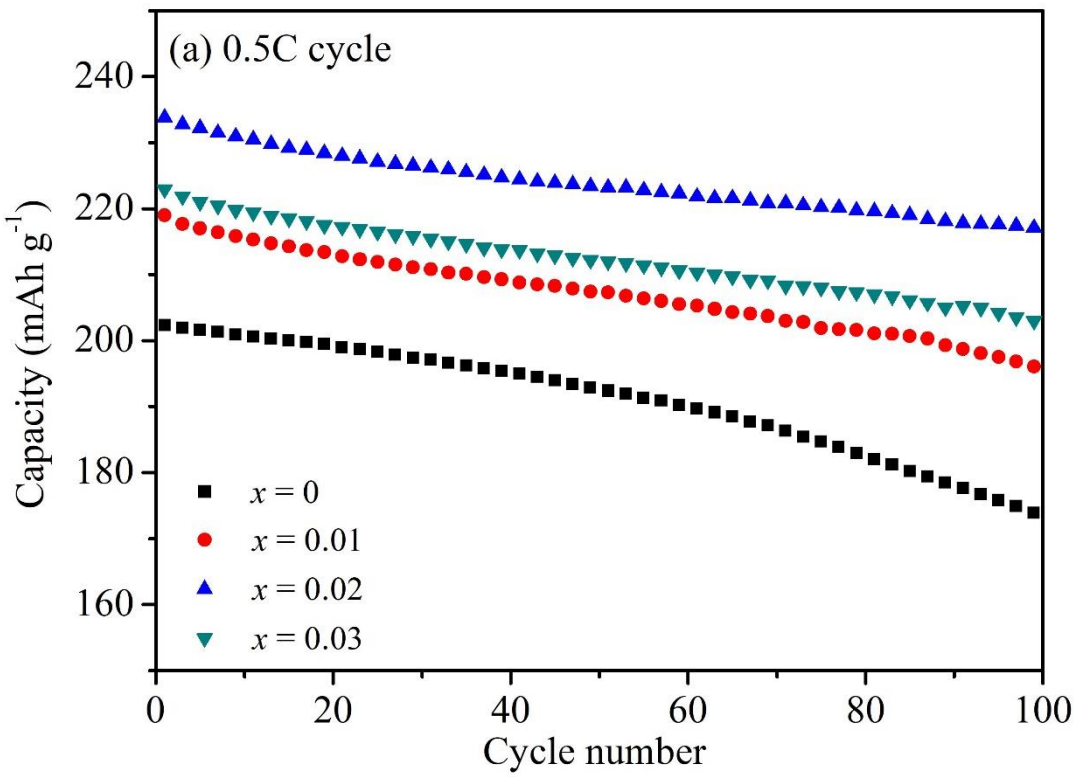

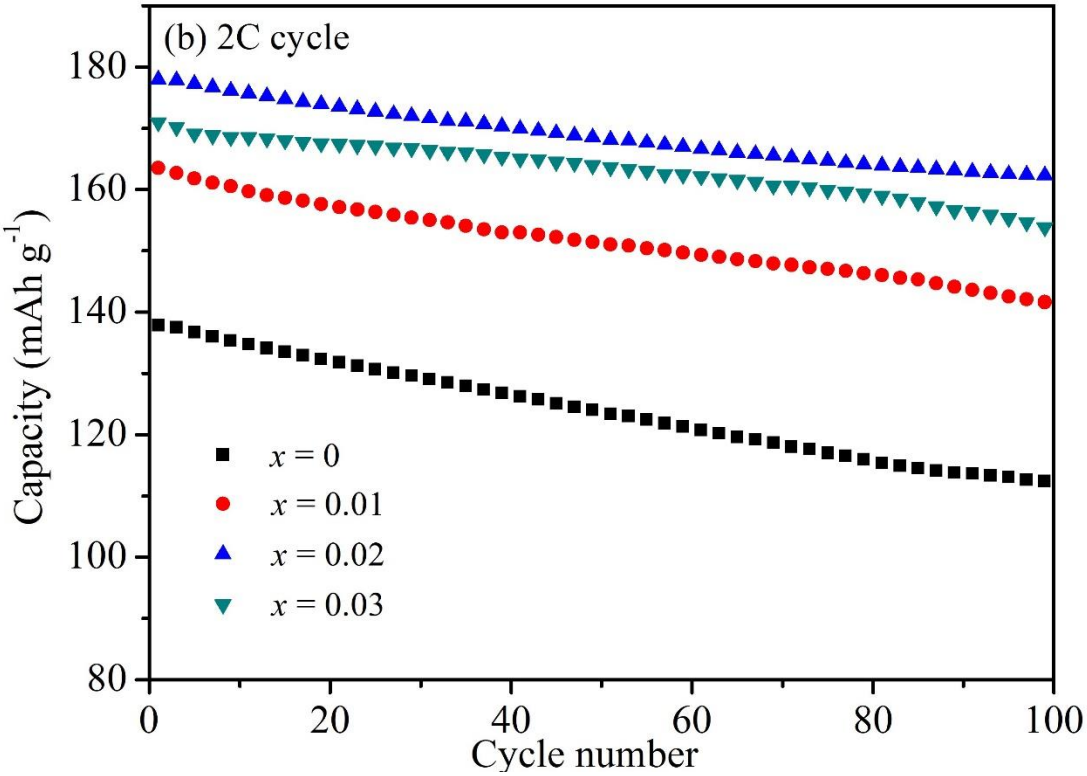

Figure 5. Cyclic performance of the $Li_{1.20}[Mn_{0.54-x}Ni_{0.13}Co_{0.13}Ce_x]\ O_2$ (x = 0, 0.01, 0.02, 0.03) at 0.5C rate(a); 2C rate(b).

The cycling stabilities for the pristine and Ce^{3+} doped cathodes were evaluated and the results are shown in Fig. 5. And Fig.5(a) shows the cyclic performance of the $Li_{1.20}[Mn_{0.54-x}Ni_{0.13}Co_{0.13}Ce_x]\ O_2$ (x = 0, 0.01, 0.02, 0.03) at 0.5C rate. The cyclic profiles have demonstrated that the Ce^{3+} doping can not only enhance the discharge capacity of cathodes, but also maintain the cyclic stability. Apparently, the pristine cathode suffers from fast capacity decay during cycling process. It delivers an initial discharge capacity of 202.3 mAh g^{-1}, but only a capacity of 173.4 mAh g^{-1} is left (85.7% of capacity retention) after 100 cycles. While the $Li_{1.20}[Mn_{0.54-x}Ni_{0.13}Co_{0.13}Ce_x]\ O_2$ (x = 0.01, 0.02, 0.03) exhibit the discharge capacity of 195.8, 217.0 and 202.8 mAh g^{-1}, respectively, corresponding to the high capacity retention of 89.4%, 92.8% and 91.0%, much higher than that of the pristine one. Besides, the high rate cycling using should be considered when applied in the people daily life. Fig.5(b) shows the cyclic performance of the $Li_{1.20}[Mn_{0.54-x}Ni_{0.13}Co_{0.13}Ce_x]\ O_2$ (x = 0, 0.01, 0.02, 0.03) at 2C rate. Generally, the higher the current density, the larger the mechanical strain and stress within cathode particles will appear [29], which can lead to the more severe structure destruction and capacity fade during high-rate charge and discharge process. In comparison with the 0.5C rate, it can be obviously observed that the all as-prepared samples have demonstrated the more severe capacity decay. For the pristine sample, it exhibits a first discharge capacity of 137.8 mAh g^{-1}, and decreases to 112.3 mAh g^{-1} after 100 cycles, with a capacity retention of only 81.5%. Comparatively, the $Li_{1.20}[Mn_{0.52}Ni_{0.13}Co_{0.13}Ce_{0.02}]O_2$ shows the optimal cycling stability at 2C high rate among the four samples. The initial discharge capacity of $Li_{1.20}[Mn_{0.52}Ni_{0.13}Co_{0.13}Ce_{0.02}]O_2$ is 177.9 mAh g^{-1}, and it still remains 162.2 mAh g^{-1} after 100 cycles, with a much higher capacity retention of 91.2%. The superior cyclic performance of Ce^{3+} doped cathode is mainly ascribed that the Ce^{3+} doping could not only lower the cation mixing between Li^+ and Ni^{2+}, but

also suppress the loss of lattice oxygen, which both contribute to enhancing the cathode structure stability during cycling. And Table 5 shows the rate capacity and cycling performance of 1 wt% CeO_2@$Li(Li_{0.17}Ni_{0.2}Co_{0.05}Mn_{0.58})O_2$ [17], 2 wt.% CeF_3@$Li_{1.2}Mn_{0.54}Ni_{0.13}Co_{0.13}O_2$ [18] described in literature and $Li_{1.20}[Mn_{0.52}Ni_{0.13}Co_{0.13}Ce_{0.02}]O_2$ in the work. In comparison with 2 wt.% CeF_3@$Li_{1.2}Mn_{0.54}Ni_{0.13}Co_{0.13}O_2$, the $Li_{1.20}[Mn_{0.52}Ni_{0.13}Co_{0.13}Ce_{0.02}]O_2$ delivers the larger discharge capacity at 2C high rate. As for the cycling performance, the Ce^{3+}-doped cathode has demonstrated the obvious superior than those of the 1 wt% CeO_2@$Li(Li_{0.17}Ni_{0.2}Co_{0.05}Mn_{0.58})O_2$ and 2 wt.% CeF_3@$Li_{1.2}Mn_{0.54}Ni_{0.13}Co_{0.13}O_2$.

Table 5. Comparison of high rate capacity and Cycling performance for 1 wt% CeO_2@$Li(Li_{0.17}Ni_{0.2}Co_{0.05}Mn_{0.58})O_2$, 2 wt.% CeF_3@$Li_{1.2}Mn_{0.54}Ni_{0.13}Co_{0.13}O_2$ and $Li_{1.20}[Mn_{0.52}Ni_{0.13}Co_{0.13}Ce_{0.02}]$ O_2.

Cathode	Discharge capacity at 2C rate (mAh g^{-1})	Cycling performance (%)
1 wt% CeO_2@$Li(Li_{0.17}Ni_{0.2}Co_{0.05}Mn_{0.58})O_2$	192.0	90.8 (1C after 80 cycles)
2 wt.% CeF_3@$Li_{1.2}Mn_{0.54}Ni_{0.13}Co_{0.13}O_2$	147.4	91.7 (0.1C after 50 cycles)
$Li_{1.20}[Mn_{0.52}Ni_{0.13}Co_{0.13}Ce_{0.02}]$ O_2	176.8	92.8 (0.5C after 100 cycles)

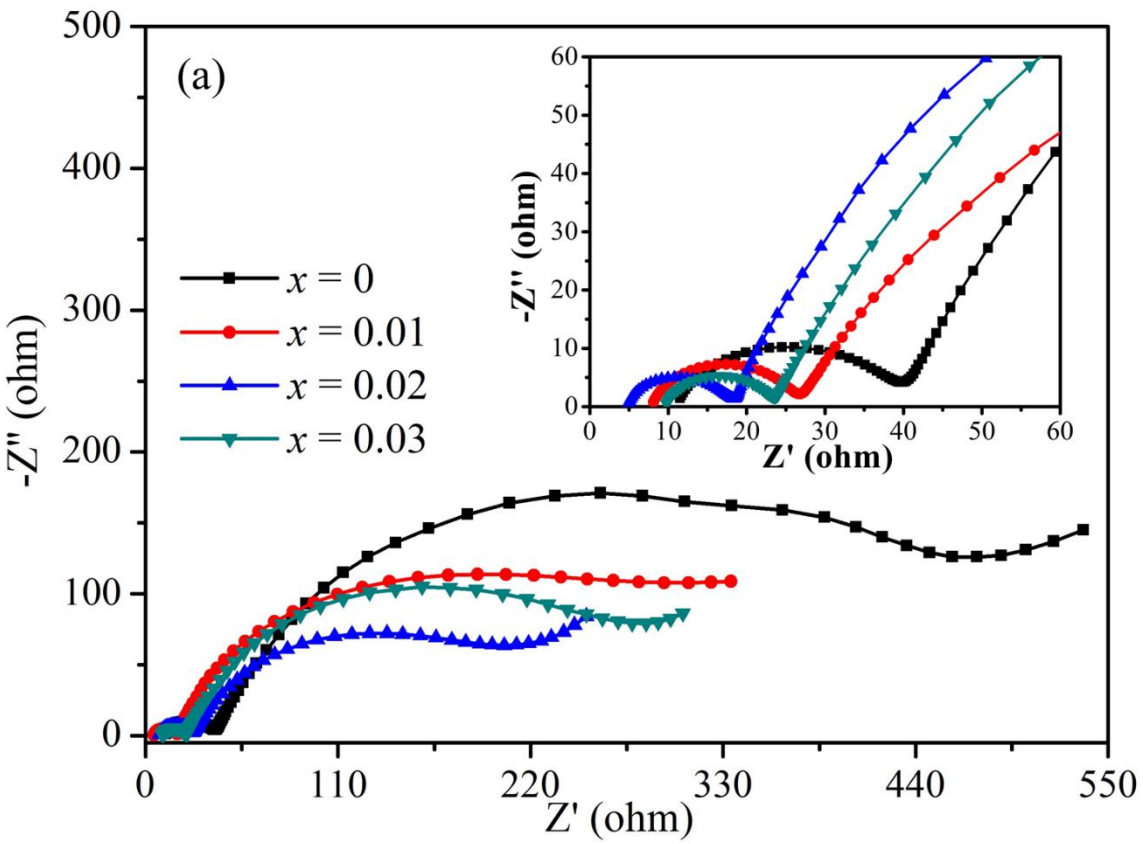

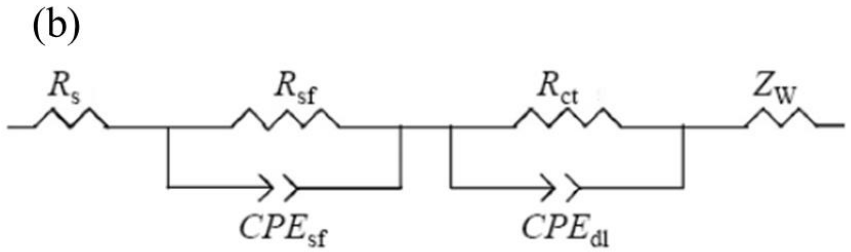

Figure 6. Nyquist plots of the $Li_{1.20}[Mn_{0.54-x}Ni_{0.13}Co_{0.13}Ce_x]$ O_2 (x = 0, 0.01, 0.02, 0.03) electrodes at a charge state of 4.8 V after 100 cycles (a); the equivalent circuit used to fit the measured impedance spectra (b).

To further understand the effects of Ce^{3+} doping on the electrochemical properties of the $Li_{1.20}[Mn_{0.54-x}Ni_{0.13}Co_{0.13}Ce_x]$ O_2 (x = 0, 0.01, 0.02, 0.03), the EIS measurement is performed to investigate the kinetic parameters of Lithium ions intercalation/deintercalation between the pristine and Ce^{3+} doped samples. Fig.6 shows the Nyquist plots of the $Li_{1.20}[Mn_{0.54-x}Ni_{0.13}Co_{0.13}Ce_x]$ O_2 (x = 0, 0.01, 0.02, 0.03) electrodes at a charge state of 4.8 V after 100 cycles. The Nyquist plots of all cathodes are composed of a depressed semicircle in the highest frequency region, a distensible semicircle in the high to medium frequency region and a quasi-straight line in the low frequency region. All Nyquist plots have been fitted by an equivalent circuit model, as seen in Fig. 6(b). And R_s represents the ohmic resistance of whole cell (the intercept of the semicircle in the highest frequency region with the real axis (Z')), R_{sf} represents the impedance of Li^+ migration across the SEI film (the semicircle at high-frequency), R_{ct} represents the charge transfer resistance (the semicircle in the high to medium frequency region), and Z_w represents the impedance of Li^+ diffusion in the bulk (the quasi-straight line in the low frequency region) [30]. The fitting results of all cathodes have been shown in Table6.

Table 6. EIS fitting data for $Li_{1.20}[Mn_{0.54-x}Ni_{0.13}Co_{0.13}Ce_x]$ O_2 (x = 0, 0.01, 0.02, 0.03) at 4.8V after 100 cycles

Sample	R_s	R_{sf}	R_{ct}
x = 0	20.6	56.9	452.8
x = 0.01	16.7	49.8	368.6
x = 0.02	12.5	35.6	298.5
x = 0.03	14.9	42.8	338.9

It can be unambiguously seen that the values of R_s, R_{sf} and R_{ct} for the pristine are all larger than those of the Ce^{3+} doped samples, especially the values of R_{ct}, meaning the larger charge transfer resistance. Therefore, the high rate performance and cyclic stability have been obtained for the Ce^{3+} doped cathodes, which is mainly attributed to the restriction of the enlargement for the charge transfer resistance by Ce^{3+} doping.

4. CONCLUSION

A series of Ce^{3+} doped $Li_{1.20}[Mn_{0.54}Co_{0.13}Ni_{0.13}]O_2$ cathode materials have been synthesized by using the traditional co-precipitation method. The Mn^{4+} sites are successfully substituted by the Cerium

ions with different amounts, which is favorable to restrict the loss of the lattice oxygen and cation mixing between Ni^{2+} and Li^{+}. The electrochemical measurements have demonstrated the Ce^{3+} doping can not only enhance the initial coulombic efficiency and discharge capacities at high rates, but also maintain the cyclic stability during cycling. The initial coulombic efficiency is enhanced from 71.9% to 74.1% and 79.4%, then decreased to 77.7% with the increasing of Ce^{3+} doping amount for the $Li_{1.20}[Mn_{0.54-x}Ni_{0.13}Co_{0.13}Ce_x]\ O_2$ (x = 0, 0.01, 0.02, 0.03). In addition, the Ce^{3+} doped cathodes exhibit the obvious enhanced rate performance than that of the pristine one owing to the fast speed of Lithium ions migration by the Ce^{3+} doping modification. Particularly, the $Li_{1.20}[Mn_{0.52}Ni_{0.13}Co_{0.13}Ce_{0.02}]O_2$ delivers a discharge capacity of 43.9 $mAhg^{-1}$ higher than that of the pristine one at 5C rate, and also retains a capacity retention of 97.3% when cycled at 0.1C rate again. Besides, an improved capacity retention of 92.8% after 100 cycles at 0.5C rate is acquired for $Li_{1.20}[Mn_{0.52}Ni_{0.13}Co_{0.13}Ce_{0.02}]O_2$, while $Li_{1.20}[Mn_{0.54}Ni_{0.13}Co_{0.13}]O_2$ only delivers a capacity retention of 85.7%. And when the cycling current density increases to 2C high rate, the superiority of cyclic stability for the $Li_{1.20}[Mn_{0.52}Ni_{0.13}Co_{0.13}Ce_{0.02}]O_2$ has been amplified, and it delivers a high capacity retention of 91.2%, much larger than that (81.5%) of the pristine one. The EIS results have further indicated the Ce^{3+} doping can restrict the enlargement of the charge transfer resistance during cycling. It is convinced that the Ce^{3+} doping is an excellent strategy to enhance the electrochemical properties of $Li_{1.20}[Mn_{0.52}Ni_{0.13}Co_{0.13}Ce_{0.02}]O_2$ for application of Li-ion battery.

ACKNOWLEDGEMENTS
This work was supported by the National Natural Science Foundation of China (51974119, 51774135, 51972120 and 51874131), China Postdoctoral Science Foundation (2017M612558 and 2018T110831) and Research project of Hunan Provincial Education Department (17C0641).

References

1. Y. Lu, T. Wang, Z. Tian and Q. Ye, *Int. J. Electrochem. Sci.*, 12 (2017) 8944.
2. Y. Ji, P. Zhang, M. Lin, W. Zhao, Z. Zhang, Y. Zhao and Y. Yang, *J. Power Sources*, 359 (2017) 391.
3. C.Y. Zhu, J.X. Liu, X.H. Yu, Y.J. Zhang, X.D. Jiang, P. Dong and Y.N. Zhang, *Int. J. Electrochem. Sci.*, 14 (2019) 7673.
4. L. Chen, Y. Yang, Z. Wang, Z. Lin, J. Zhang, Q. Su, Y. Chen, W. Chen, Y. Lin and Z. Huang, *J. Alloys Compd.*, 711 (2017) 462.
5. X.H. Liang, Y.C. Zhao, D. Han, J. Mao and L.X. Lan, *Int. J. Electrochem. Sci.*, 14 (2019) 717.
6. X. Wei, Y. Guan, X. Zheng, Q. Zhu, J. Shen, N. Qiao, S. Zhou and B. Xu, *Appl. Surf. Sci.*, 440 (2018) 748.
7. L.J. Chen, W.J. Feng, Z.S. Pu, X. Wang, W.X. Su, M.M. Li, C.K. Song, Z.J. Shi and Y.F. Zheng, *Int. J. Electrochem. Sci.*, 14 (2019) 8048.
8. Y. Lu, S. Shi, F. Yang, T. Zhang, H. Niu and T. Wang, *J. Alloys Compd.*, 767 (2018) 23.
9. L. Ku, Y.X. Cai, Y.T. Ma, H.F. Zheng, P.F. Liu, Z.S. Qiao, Q.S. Xie, L.S. Wang and D.L. Peng, *Chem. Eng. J.,* 370 (2019) 499.
10. D. Zhang, W. Li, N. Li, J. Qiao, Z. Ma and C. Chang, *Int. J. Electrochem. Sci.*, 13 (2018) 6402.
11. Y. Lu, S. Shi, F. Yang, T. Zhang, H. Niu and T. Wang, *J. Alloys Compd.*, 767 (2018) 23.
12. W. Pan, W. Peng, H. Guo, J. Wang, Z. Wang, H. Li and K. Shi, *Ceram. Int.*, 43 (2017) 14836.

13. B. Seteni, N. Rapulenyane, J.C. Ngila, S. Mpelane and H. Luo, *J. Power Sources*, 353 (2017) 210.
14. X. He, J. Wang, R. Kloepsch, S. Krueger, H. Jia, H. Liu, B. Vortmann and J. Li, *Nano Res.*, 7 (2013) 110.
15. X. Li, L. Zheng, Z. Zang, T. Liu, F. Cao, X. Sun, S. Sun, Q. Niu, Y. Lu, T. Ohsaka and J. Wu, *J. Alloys Compd.*, 744 (2018) 41.
16. X. Geng, H. Guo, C. Wang, M. Cheng, Y. Li, H. Zhang and H. Huo, *J. Mater. Sci.- Mater. Electron.*, 29 (2018) 19207.
17. W. Yuan, H.Z. Zhang, Q. Liu, G.R. Li and X.P. Gao, *Electrochim. Acta,* 135 (2014) 199.
18. C. Lu, H. Wu, Y. Zhang, H. Liu, B.J. Chen, N.T. Wu and S. Wang, *J. Power Sources*, 267 (2014) 682-691.
19. Y. Lu, M. Pang, S. Shi, Q. Ye, Z. Tian and T. Wang, *Sci. Rep.*, 8 (2018) 2981.
20. R.M. Yang, Y.J. Zhang, P. Dong and Y.N. Zhang, *Int. J. Electrochem. Sci.*, 13 (2018) 8116.
21. X. Chang, Q. Xu, X. Yuan, C. Lai and H. Liu, *Int. J. Electrochem. Sci.*, 12 (2017) 10071.
22. M. Xu, L. Fei, W. Lu, Z. Chen, T. Li, Y. Liu, G. Gao, Y. Lai, Z. Zhang, P. Wang and H. Huang, *Nano Energy*, 35 (2017) 271.
23. K. R. Prakasha, M. Sathish, P. Bera and A. S. Prakash, *ACS Omega*, 2 (2017) 2308.
24. G. Li, X. Liu, Y. Zhao and Z. Shao, *Int. J. Electrochem. Sci.*, 13 (2018) 7321.
25. B. Liu, Z. Zhang, M. Wu and S. Xu, *Int. J. Electrochem. Sci.*, 13 (2018) 7578.
26. Z. Shen and Dong Li, *J. Mater. Sci.- Mater. Electron.*, 28 (2017) 13257.
27. S. Hy, H. Liu, M. Zhang, D. Qian, B.J. Hwang and Y.S. Meng*, Energy Environ. Sci.*, 9 (2016) 1931.
28. Z.Q. Zou, M. Meng, L.H. Guo and Y.Q. Zha, *J. Hazard. Mater.*, 163 (2009) 835.
29. C. Lu, H. Wu, B. Chen, H. Liu and Y. Zhang, *J. Alloys Compd*., 634 (2015) 75.
30. M. Wang, M. Luo, Y. Chen, Y. Su, L. Chen and R. Zhang, *J. Alloys Compd.,* 696 (2017) 907.